LBL-11834

CONF-801103--38

Lawrence Berkeley Laboratory
UNIVERSITY OF CALIFORNIA

Physics, Computer Science & Mathematics Division

Presented at the IEEE Nuclear Science Symposium, Orlando, FL, November 5-8, 1980; and to be published in the IEEE Transactions on Nuclear Science

LIMITS TO IMAGE RECONSTRUCTION FROM RESTRICTED ANGULAR INPUT

K.C. Tam and V. Perez-Mendez

November 1980

Prepared for the U.S. Department of Energy under Contract W-7405-ENG-48

LBL-11834

LIMITS TO IMAGE RECONSTRUCTION FROM RESTRICTED ANGULAR INPUT

K. C. TAM
GENERAL ELECTRIC COMPANY
CORPORATE RESEARCH AND DEVELOPMENT CENTER
BLDG. 37 ROOM 5030
SCHENECTADY, NEW YORK 12345

V. PEREZ-MENDEZ
LAWRENCE BERKELEY LABORATORY, BERKELEY, CALIFORNIA 94720 AND
RADIOLOGY DEPARTMENT, UNIVERSITY OF CALIFORNIA,
SAN FRANCISCO, CALIFORNIA 94143

ABSTRACT

Distortion in an object due to the unavailability of some Fourier components in a cone-shaped region is analyzed. The results throw light on the factors that limit the accuracy in reconstructing objects from limited-angle input in practice. It is also shown that norm- or entropy-related reconstruction methods are not expected to improve the fidelity of the reconstructed images; only more a priori knowledge of exact nature on the object can serve this purpose.

INTRODUCTION

In many radiation imaging applications, such as X-ray computerized tomography, nuclear medicine, and electron microscopy, it may be necessary or advantageous to image an object from a restricted angular range. It has been shown that in such cases the Fourier components of an object that can be measured directly are those outside a cone-shaped region in the Fourier space [1,2]. In principle, all the missing Fourier components can be recovered completely if the object is known to be finite in extent [1,2]. In this paper we explore the practical limits to the recovering operations. In conformity with our previous terminology, we shall refer to the region in Fourier space where the Fourier components of an object are measured directly as the "allowed cone", and where they are not known as the "missing cone".

Information Contained in Limited-Angle Data

In this section we derive an expression for the distorted object obtained by setting the Fourier components of an object in the missing cone to zero, which throws light on the practical limits to restricted-angle reconstructions.

An iteration algorithm has been proposed in our previous papers [1,2] to recover the missing-cone Fourier components of an object distribution. The algorithm is shown in Fig. 1. After initially setting its missing-cone components to zero, the object is manipulated back and forth between the object space ($\underline{x}$-space) and the Fourier space ($\underline{k}$-space) via Fourier transformations, being corrected in each step by its known finite spatial extent R_b and the measured Fourier components inside the allowed cone R_a which are schematically shown in Fig. 2. The iteration scheme can be formulated in terms of two operators A and B opearing on any Fourier transformable function f defined in the Fourier space. A and B are defined as follows:

$$Af = \chi_A f$$

$$Bf = F^{-1}\chi_B F f$$

where F and F^{-1} represent the Fourier transformation and its inverse; χ_A, χ_B are, respectively, the characteristic functions of the allowed cone, R_a, in Fourier space and of the object region, R_b, in object space, and are defined as:

$$\chi_A(\underline{k}) = \begin{cases} 1 & \underline{k} \in R_a \\ 0 & \underline{k} \notin R_a \end{cases}$$

$$\chi_B(\underline{x}) = \begin{cases} 1 & \underline{x} \in R_b \\ 0 & \underline{x} \notin R_b \end{cases}$$

In terms of these operators the reconstructed image $R^{(n)}(\underline{k})$ in Fourier space after n steps of iteration can be represented as:

$$R^{(1)}(\underline{k}) = BAR(\underline{k}),$$

$$R^{(n)}(\underline{k}) = BAR(\underline{k}) + (I-BA)R^{(n-1)}(\underline{k}) \qquad (1)$$

$$\text{for } n = 2, 3, 4, \ldots\ldots$$

where $R(\underline{k})$ is the Fourier transform of the object. It has been shown in [3] that equation (1) can be written in terms of the orthonormal set of eigenfunctions $\{\psi_i(\underline{k})\}$ of the composite operator BA and the corresponding set of eigenvalues $\{\lambda_i\}$,

$$R^{(n)}(\underline{k}) = \sum_i a_i (1-(1-\lambda_i)^n)\psi_i(\underline{k}), \quad 0 < \lambda_i < 1 \qquad (2)$$

where the a_is are the expansion coefficients of the object $R(\underline{k})$ in terms of the ψ_is,

$$R(\underline{k}) = \sum_i a_i \psi_i(\underline{k}) \qquad (3)$$

Now from equation (1) the image after the first iteration, $R^{(1)}(\underline{k})$, is the distorted object obtained by setting the missing-cone Fourier components of the object to zero, Fourier transforming to the object space, and then resetting the values outside the known object region to zero. From equation (2) this distorted object is given by:

$$R^{(1)}(\underline{k}) = \sum_i \lambda_i a_i \psi_i(\underline{k}) \qquad (4)$$

Equation (4) shows that each eigenfunction component $a_i\psi_i(\underline{k})$ of the object is attenuated by a factor λ_i if the Fourier components of the object in the missing cone are set to zero. This result agrees well with the meaning of the λ_is, namely, λ_i is the ratio of the energy of the function $\psi_i(\underline{k})$ in R_a to the total energy of $\psi_i(\underline{k})$ [4].

Equation (4) also shows that in principle an object $R(\underline{k})$ can be inverted from the distorted object $R^{(1)}(\underline{k})$ with information only in the allowed cone: each eigenfunction coefficient a_i of $R(\underline{k})$ is obtained by dividing the corresponding coefficient of $R^{(1)}(\underline{k})$ by λ_i. This inversion process is possible for every eigenfunction component, since all the eigenvalues are non-zero. In other words, all the information on an object is, in principle, contained in its Fourier

components in the allowed cone. We note that a relation similar to equation (4) was also derived in a recent paper by Rushforth and Frost [5] for one-dimensional band-limited signals.

In practice, however, the eigenfunction components corresponding to the small eignevalues are very difficult to recover because of the instability due to noise amplification by $1/\lambda_i$. Figure 3 shows a plot of the spectra of λ_i for various half-angles of the allowed cone for a 9 pixels by 9 pixels square-shaped object boundary in a 21 x 21 reconstruction region. Each spectrum can be roughly divided into two regions: one in which the λ_is are close to unity, and the other in which the λ_is are close to zero. It is these small λ_is which make the inversion problem unstable in the presence of noise.

Even in the hypothetical situation of noise free input data, some of the eigenfunction components corresponding to very small eigenvalues are lost in practical computation. This is due to the fact that all computing devices have a finite accuracy δ, which means that if $\lambda_i a_i < \delta$ it cannot be registered, and consequently a_i cannot be determined by any means. Such indeterminacy is to be expected from the meaning of λ_i: the eigenfunction component $a_i\psi_i(\underline{k})$ cannot be recovered if it is too weakly represented in the data as to be of any practical use. Similar conclusion was also arrived at by Klug and Crowther [6].

As an illustration consider the above mentioned Fourier iteration algorithm in Fig. 1. The truncation error $E_t^{(n)}(\underline{k})$ in terminating the iteration after n steps is obtained from equation (2):

$$E_t^{(n)}(\underline{k}) = R^{(n)}(\underline{k}) - R(\underline{k})$$
$$= -\sum_i a_i (1 - \lambda_i)^n \psi_i(\underline{k}).$$

For the λ_is close to one the error coefficients $(1-\lambda_i)^n$ approach zero rapidly as n increases; whereas for the λ_is close to zero it will take a very large number n of iterations for $(1-\lambda_i)^n$ to converge to zero. For those λ_is below the accuracy of the computing device, $(1-\lambda_i)^n$ always stays at 1 and does not converge at all, which means that the corresponsing component $a_i\psi_i(\underline{k})$ cannot be recovered. In such case the iteration algorithm automatically sets these components to zero, from equation (2), which is the most reasonable thing to do in the absence of any information.

Norm Minimization and Entrophy Maximization

The problem of determining the eigenfunction components corresponding to very small eigenvalues can be likened to the missing-cone problem which we start with. The Fourier components in the missing cone are not known initially, but, in principle, the additional information on the finite spatial extent of the object enables these missing Fourier components to be calculated from those in the allowed cone. Similarly, the indeterminate eigenfunction components corresponding to very small eigenvalues can be recovered, and thus the fidelity of limited-angle reconstructions improved, only if more a priori knowledge or constraints on the object other than its finite extent and location are available. For example, if it is known that an object has n-fold rotation symmetry, projections in an angular range of π/n (instead of full π angle) will suffice to reconstruct it completely. Another example occurs in determining the refractive index (heat distribution) around a wire carrying current where the diffusion equation holds [7]. However, except for the constraint of positivity which has been shown to be of little help in reconstructing extended objects [8], no other constraints of an exact nature are available for general objects.

There are a number of algorithms which attempt to reconstruct an object by imposing some extremum property on the object as additional information. Among these algorithms are norm minimization [9] and entropy maximization [10,11]. The constraints of minimum norm and maximum entropy are not exact descriptions of the object, rather they are probabilistic in nature. In this section we investigate the possibility of using these constraints to recover the undetermined coefficients a_is of the small-eigenvalue components in limited-angle reconstruction.

The significance of the minimum norm solution is that it is also the minimum variance solution consistent with the data. This can be seen by considering

$$\int(\rho(\underline{r}) - \bar{\rho})^2 d^2r$$
$$= \int\rho(\underline{r})^2 d^2r - \bar{\rho}^2 x \text{ (object area)}$$

where $\bar{\rho}$ is the mean density of the object distribution $\rho(\underline{r})$.

Minimum norm reconstructions thus presuppose that reconstructed images containing wide ranges of density values are unlikely. From Parseval's theorem and equation (3), the norm of $\rho(\underline{r})$ can be written as

$$\int\rho(\underline{r})^2 d^2r = \int|R(\underline{k})|^2 d^2k$$
$$= \sum_i |a_i|^2 \qquad (5)$$

Equation (5) indicates that setting the undetermined coefficients a_is of the small-eigenvalue components to zero yields the minimum norm solution subject to the constraints of the measured data and the finite object boundary. Clearly this solution may not be the true solution.

The entropy S of an object distribution $\{\rho_i\}$ is defined as [12]:

$$S = -\sum_i \frac{\rho_i}{T} \log \frac{\rho_i}{T}$$

where $T = \sum_i \rho_i$ is the total object density. This quantity is a measure of the degree of randomness, and hence the probability of occurrence, of an object distribution [13]. Algorithms of object reconstruction through entropy maximization are based on the assumption that the most probable object distribution is the one that possesses maximum entropy subject to some given constraints, such as projection data at some angles.

We have plotted the ratio of the rms error to mean density and the entropy of some reconstructed images of a 2-D phantom. The phantom, shown in Fig. 4, is a diamond-shaped object in a 32 x 32 reconstruction region; the densities of the boundary, the interior, and the hot spot in the middle are 2, 1, and 4 respectively. The object was reconstructed from its Fourier components in the allowed cone through the Fourier iteration algorithm. The results are shown in Fig. 5-9 for the cases where the half-angle of the allowed cone equals $\tan^{-1}(0.5)$, $\tan^{-1}(1)$, $\tan^{-1}(2)$, and $\tan^{-1}(4)$ respectively. The rms error converges to a steady level after about 20 iterations in all

cases; the magnitude of the residual rms error decreases with increase in the allowed-cone angle. The behavior of these rms error curves can be expected from the shape of the spectra of eigenvalues shown in Fig. 3. As mentioned in the previous section, the finite residual error is due to the small eigenvalues whose error terms $a_i(1-\lambda_i)^n\psi_i(\underline{k})$ approach zero very slowly or not at all. As the allowed cone angle increases, Fig. 3 shows that the proportion of small eigenvalues decreases, so does the residual error.

As for the entropy of the reconstructed images, it increases rapidly with decrease in rms error during the first ~20 iterations, and then converges to the entropy value of the original object after the rms error settles to a steady level regardless of the magnitude of the residual rms error. Since the residual error is caused by the small eigenvalues, these results show that the entropy of the reconstructed images is insensitive to the small-eigenvalue components. The reason for this insensitivity is discussed in Appendix A. The implication, however, is quite clear: it would be very difficult to recover the small-eigenvalue components by any entropy-related reconstruction methods.

Conclusion

We have shown that due to limitations in computing accuracy some information is not recoverable in reconstructing an object from restricted angular input. This is true even in the ideal case when there is no error in input data. The fidelity of reconstructed images can only be improved if more a priori information on the object other than its finite spatial extent and location is available. We have also shown that norm- or entropy-related methods are not likely to produce such improvements.

Acknowledgements

This work was supported by the Physics, Computer Science and Mathematics Division of Lawrence Berkeley Laboratory, United States Department of Energy under contract No. W-7405-ENG-48.

Appendix A

The reason for the insensitivity of the entropy of reconstructed images to the small-eigenvalue components can be understood with the help of Fig. 1. Assume the center lines of the allowed cone and the missing cone are oriented along the k_x-axis and the k_z-axis respectively. Let ρ_i represent the object density at pixel i recontructed from limited-angle information through the Fourier iteration algorithm, and $\Delta\rho_i$ be the contribution to the density at pixel i from the very-small-eigenvalue components that cannot be determined and hence set to zero. Thus $\{\rho_i + \Delta\rho_i\}$ represents the true object distribution. The distribution $\{\Delta\rho_i\}$ is essentially made up of low-k_x high-k_z Fourier components since they are furthermost away from the allowed cone and hence least affected by the information there. Consequently $\{\rho_i\}$ is deficient in low-k_x high-k_z Fourier componets, and thus the two distributions $\{\rho_i\}$ and $\{\Delta\rho_i\}$ are uncorrelated.

Assume $\{\rho_i\}$ is normalized, i.e. $\Sigma\rho_i = 1$, it then follows $\{\rho_i + \Delta\rho_i\}$ is also normalized since $\Sigma\Delta\rho_i = 0$. The entropy S of the object and the entropy S' of the reconstructed image are given by

$$S = -\sum_i(\rho_i + \Delta\rho_i)\log(\rho_i + \Delta\rho_i)$$

$$S' = -\sum_i \rho_i \log \rho_i$$

Their difference is

$$S - S' = -\sum_i \Delta\rho_i \log \rho_i$$

Since $\{\rho_i\}$, $\Delta\rho_i$ are uncorrelated, it is reasonable that $\{\Delta\rho_i\}$ and $\{\log \rho_i\}$ are also uncorrelated, thus

$$\sum_i \Delta\rho_i \log \rho_i = 0$$

and

$$S = S'$$

References

1. Tam, K. C., Perez-Mendez, V., and Macdonald, B., LBL-8539.
2. Tam, K. C., Perez-Mendez, V., and Macdonald, B., IEEE Trans. Nucl. Sci., NS-26 (1979) 2797.
3. Tam, K. C., Perez-Mendez, V., and Macdonald, B., IEEE Trans. Nucl. Sci., NS-27 (1980) 445.
4. Slepian, D., Bell Syst. Tech. J., 43 (1964) 3009.
5. Rushforth, C. K., and Frost, R. L. , Proceedings of the 1980 International Optical Computing Conference, Washington, D. C., April 8-9, 1980.
6. Klug, A., and Crowther, R.A., Nature, 238 (1972) 435.
7. Radulovic, P. T.,and Vest, C.M., Digest of Papers, Topical Meeting on Image Processing for 2-D and 3-D Reconstruction from Projections: Theory and Practice in Medicine and the Physical Sciences, Stanford University, Palo Alto, California, August 4-7, 1975.
8. Tam, K. C. , Perez-Mendez, V., Proceedings of the 1980 International Optical Computing Conference, Washington, D.C., April 8-9, 1980; also to be published in Optical Engineering.
9. Kashyap, R. L.,and Mittal, M.C., IEEE Trans. Comput., C-24 (1975) 915.
10. Frieden, B. R., J. Opt. Soc. Amer., 62 (1972) 511.
11. Minerbo, G., Computer Graphics and Image Processing, 10 (1979) 48.
12. Shannon, C. E., and Weaver, W. 1949, The Mathematical Theory of Communication (Urbana: University of Illinois Press) p. 19.
13. Jaynes, E. T., IEEE Trans. Syst. Sci. Cybern., SSC-4 (1968) 227.

FIGURE CAPTIONS

Figure 1. Fourier transform iteration scheme for filling in missing-cone Fourier components.

Figure 2. Schematic representations of the allowed cone and the object extent.

Figure 3. Eigenvalue spectra of BA for a 2-D problem for various half-angles of the allowed cone.
Ra: oriented along the k_x-axis
Rb: a 9 pixels by 9 pixels square in a 21 x 21 reconstruction area.

Figure 4. A 2-D diamond-shaped phantom.

Figure 5. The ratio of rms error to mean density and the entropy of the reconstructed image of the diamond-shaped phantom as a function of the number of Fourier transform iterations. The half-angle of the allowed cone is $\tan^{-1}(0.5)$.

Figure 6. The ratio of rms error to mean density and the entropy of the reconstructed image of the diamond-shaped phantom as a function of the number of Fourier transform iterations. The half-angle of the allowed cone is $\tan^{-1}(1)$.

Figure 7. The ratio of rms error to mean density and the entropy of the reconstructed image of the diamond-shaped phantom as a function of the number of Fourier transform iterations. The half-angle of the allowed cone is $\tan^{-1}(2)$.

Figure 8. The ratio of rms error to mean density and the entropy of the reconstructed image of the diamond-shaped phantom as a function of the number of Fourier transform iterations. The half-angle of the allowed cone is $\tan^{-1}(4)$.

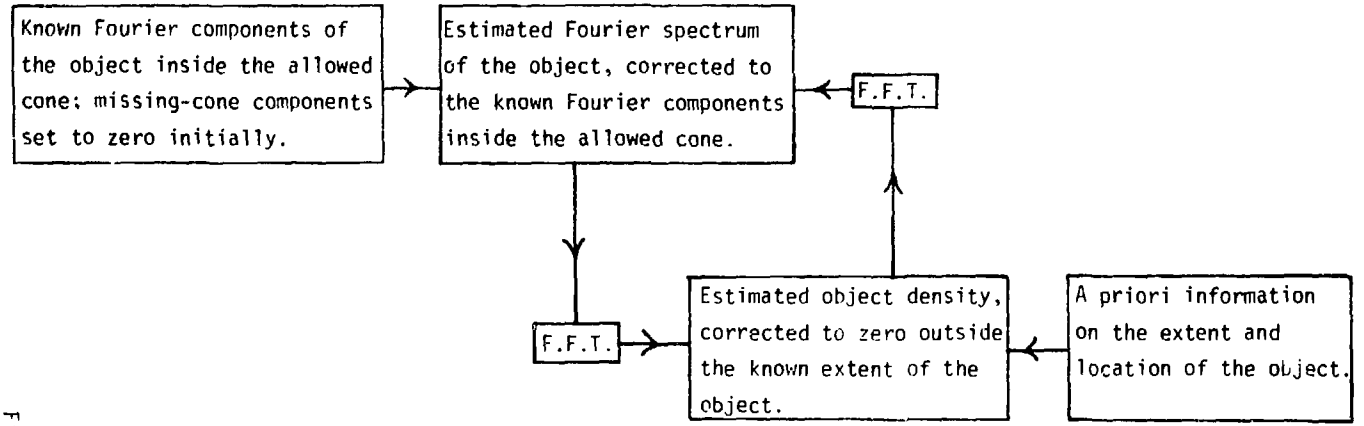
Known Fourier components of the object inside the allowed cone; missing-cone components set to zero initially.
Estimated Fourier spectrum of the object, corrected to the known Fourier components inside the allowed cone.
F.F.T.
F.F.T.
Estimated object density, corrected to zero outside the known extent of the object.
A priori information on the extent and location of the object.

Figure 1

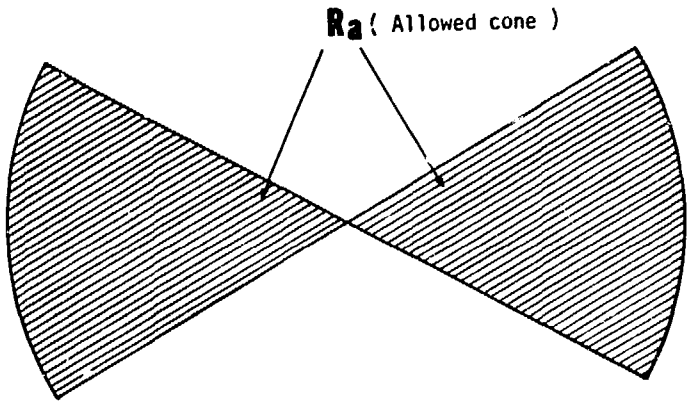

Frequency space ($\underline{k}$)

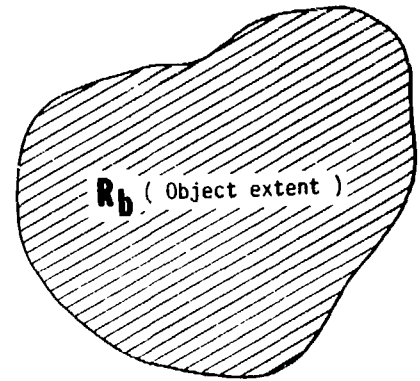

Object space ($\underline{r}$)

XBL 809-11796

Figure 2

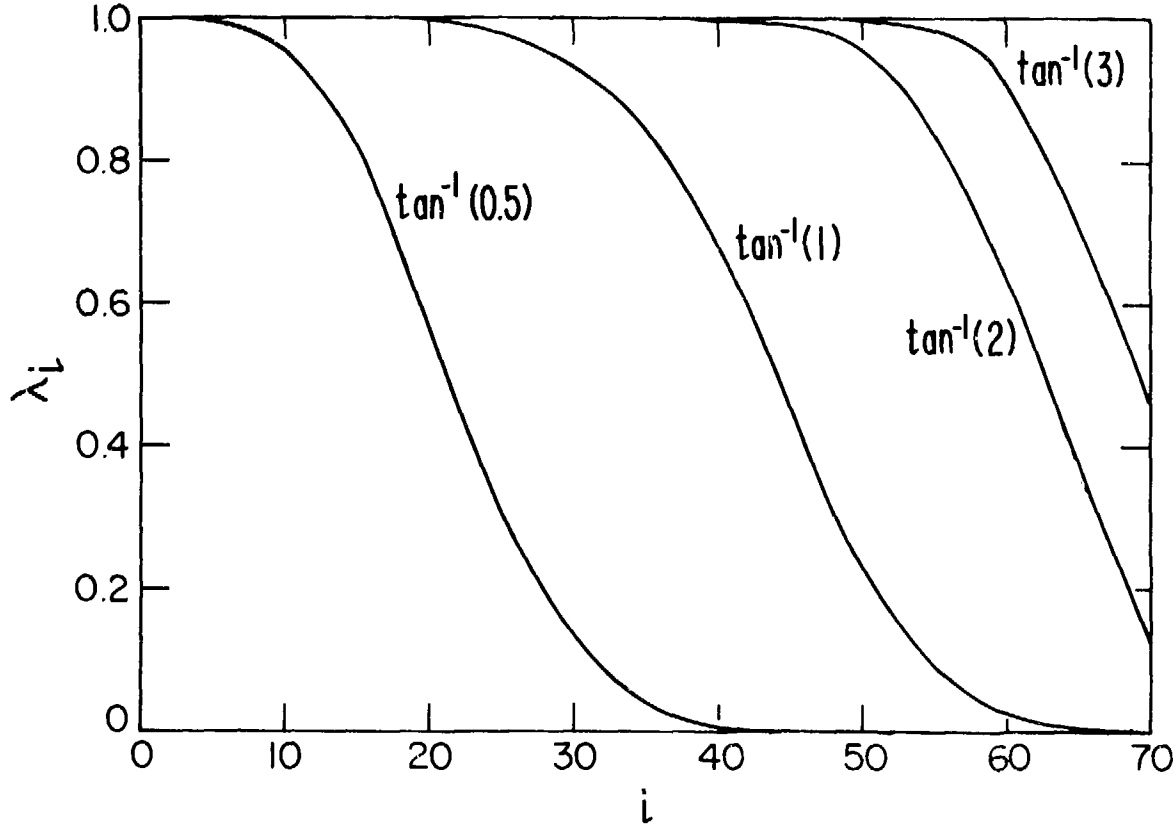

XBL 798-2379

Figure 7

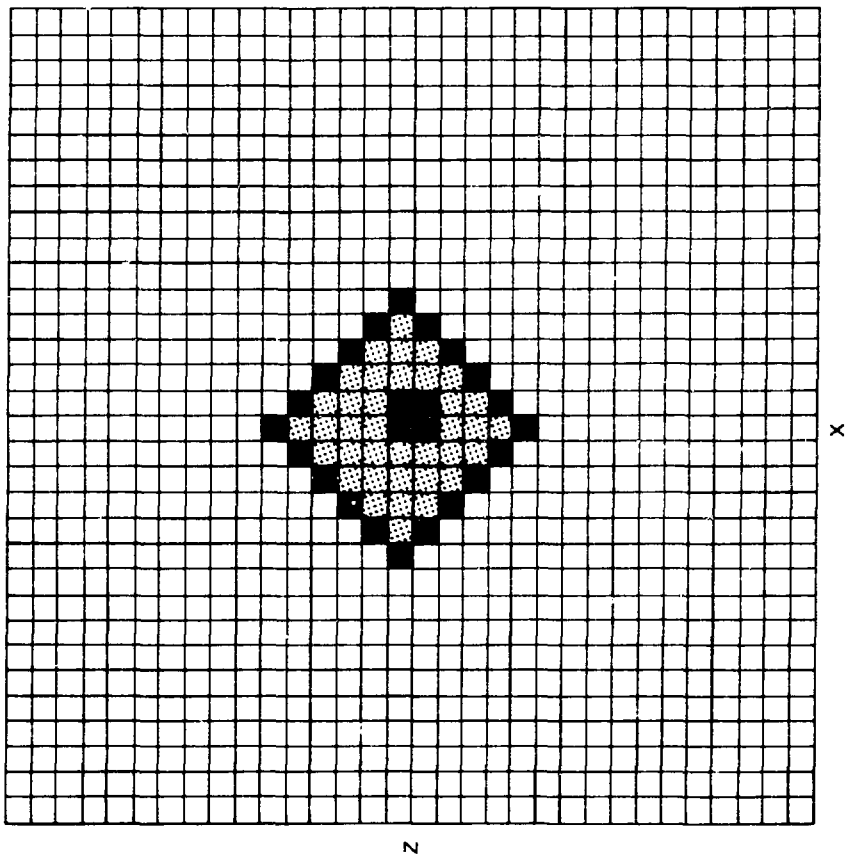

Figure 4

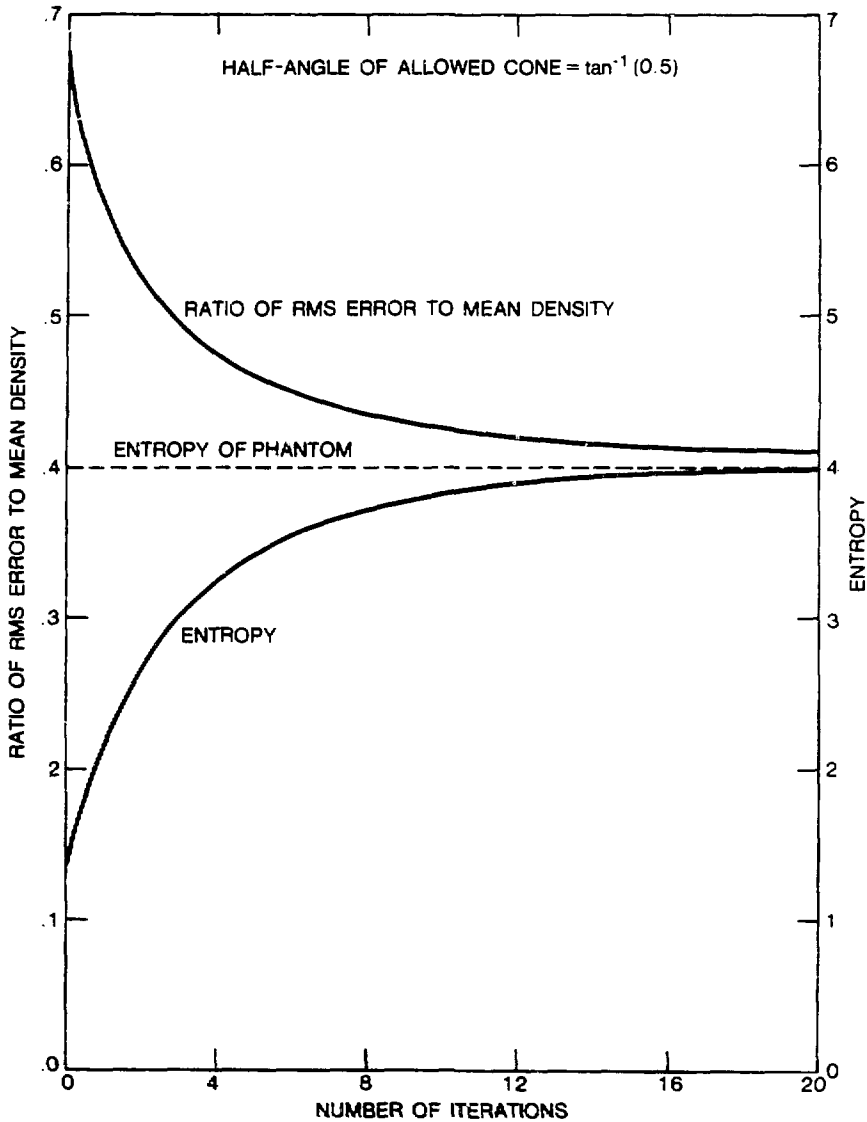
HALF-ANGLE OF ALLOWED CONE = tan^{-1} (0.5)
RATIO OF RMS ERROR TO MEAN DENSITY
ENTROPY OF PHANTOM
ENTROPY
RATIO OF RMS ERROR TO MEAN DENSITY
ENTROPY
NUMBER OF ITERATIONS
.7
.6
.5
.4
.3
.2
.1
.0
7
6
5
4
3
2
1
0
0
4
8
12
16
20

Figure 5

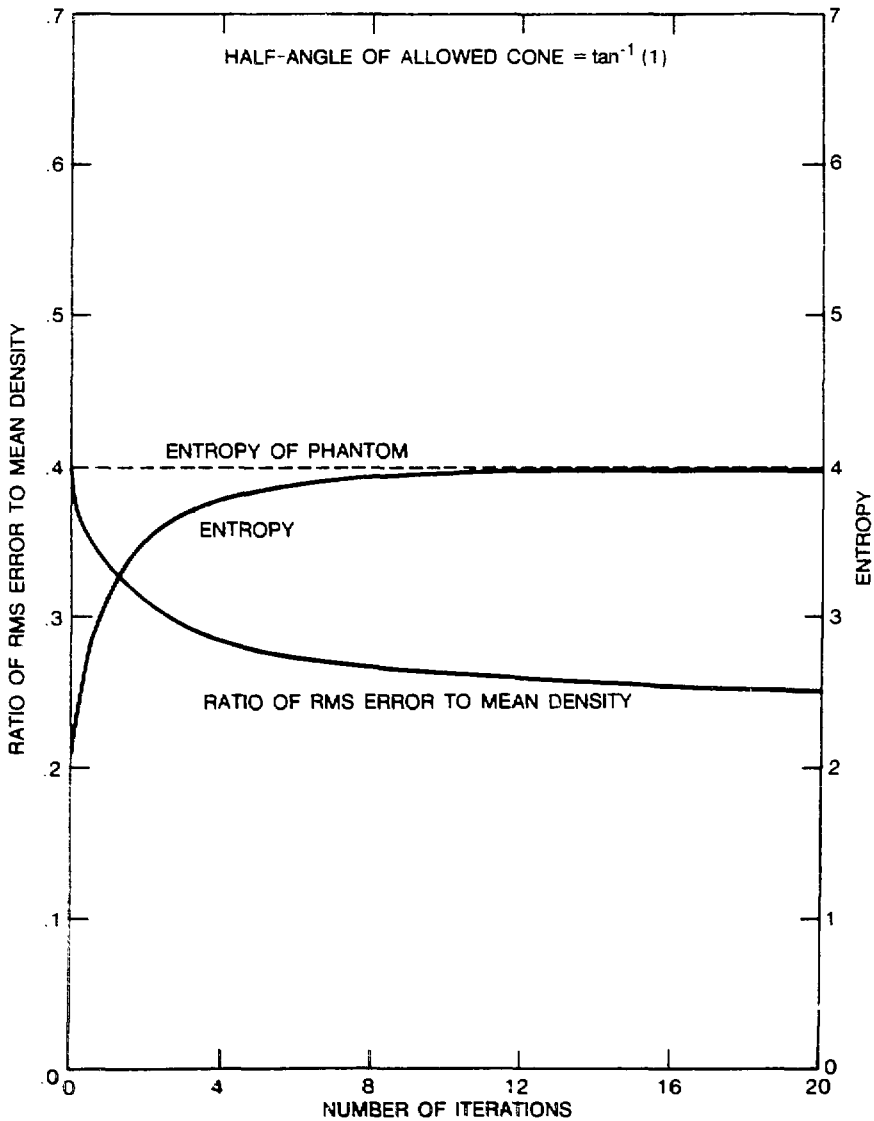
HALF-ANGLE OF ALLOWED CONE = tan^{-1} (1)
ENTROPY OF PHANTOM
ENTROPY
RATIO OF RMS ERROR TO MEAN DENSITY
RATIO OF RMS ERROR TO MEAN DENSITY
ENTROPY
NUMBER OF ITERATIONS
.7
.6
.5
.4
.3
.2
.1
0
7
6
5
4
3
2
1
0
0
4
8
12
16
20

Figure 6

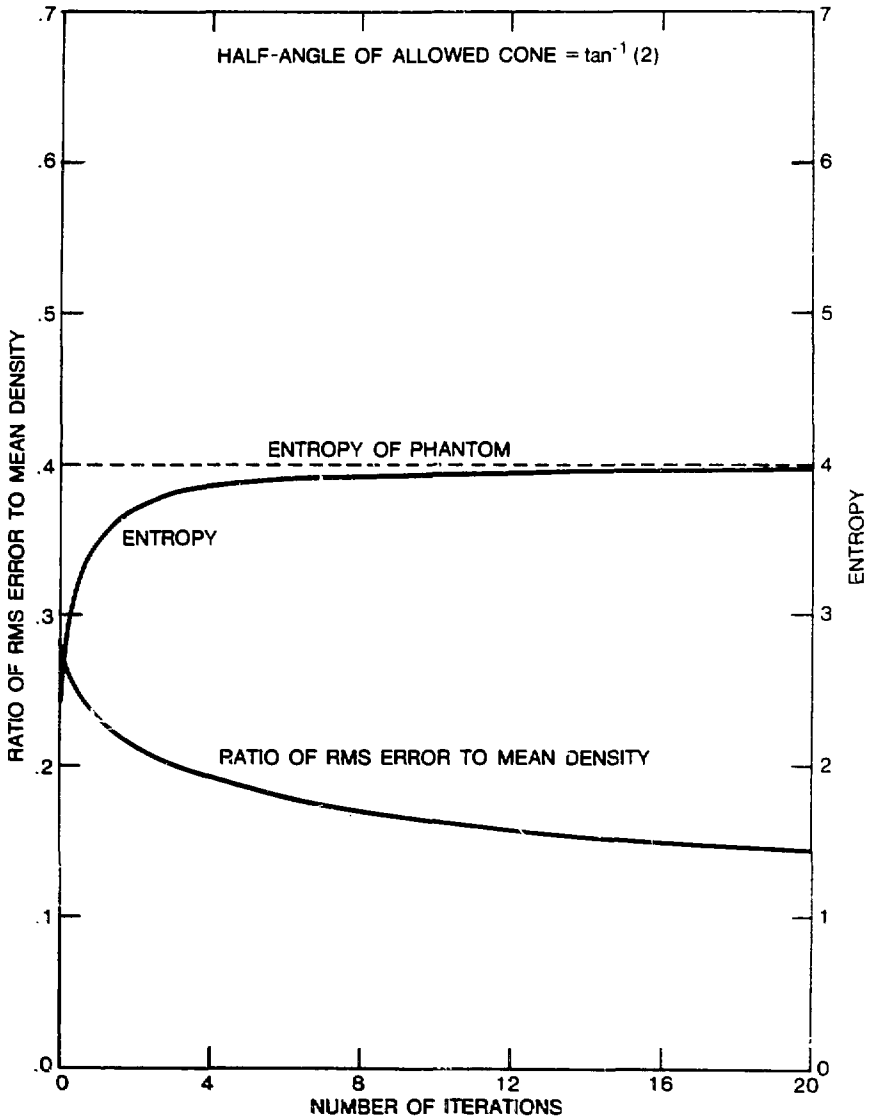
HALF-ANGLE OF ALLOWED CONE = tan^{-1} (2)
ENTROPY OF PHANTOM
ENTROPY
RATIO OF RMS ERROR TO MEAN DENSITY
RATIO OF RMS ERROR TO MEAN DENSITY
ENTROPY
NUMBER OF ITERATIONS
.7
.6
.5
.4
.3
.2
.1
.0
7
6
5
4
3
2
1
0
0
4
8
12
16
20

Figure 7

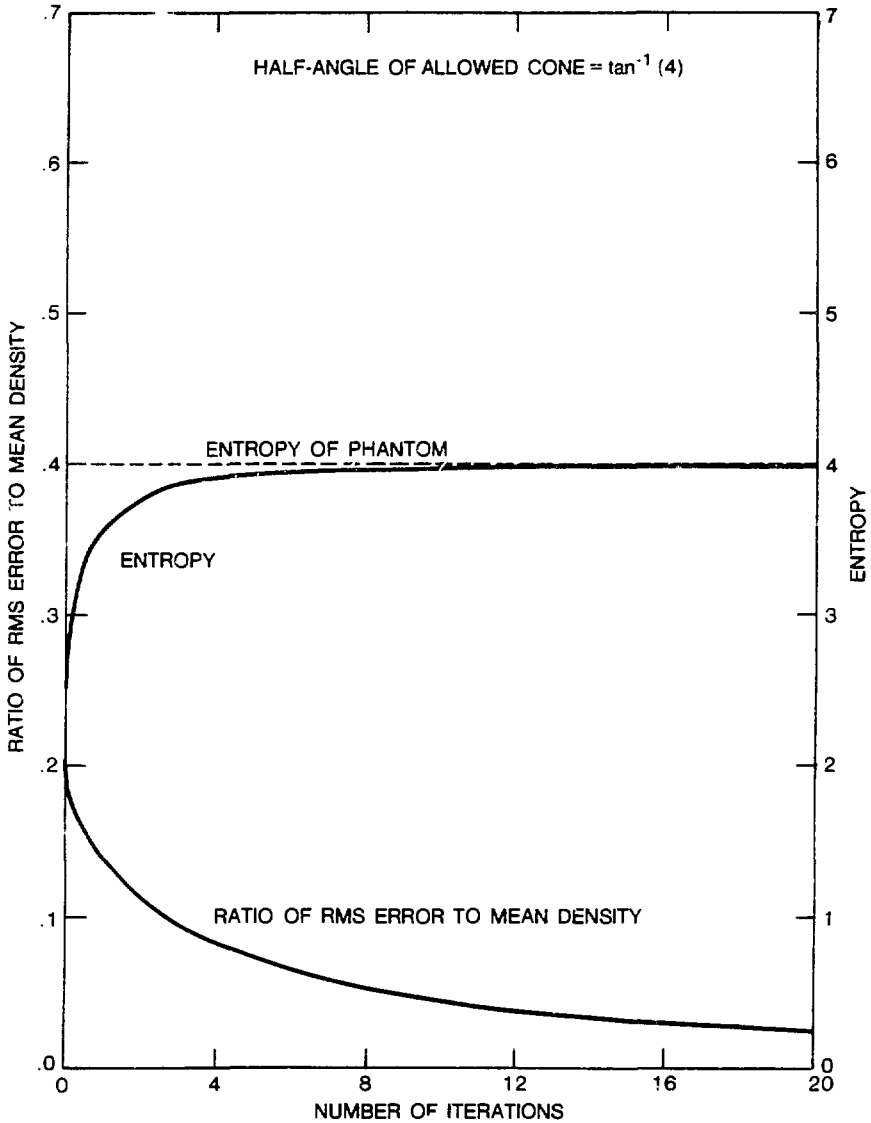
HALF-ANGLE OF ALLOWED CONE = tan^{-1} (4)
ENTROPY OF PHANTOM
ENTROPY
RATIO OF RMS ERROR TO MEAN DENSITY
RATIO OF RMS ERROR TO MEAN DENSITY
ENTROPY
NUMBER OF ITERATIONS
.7
.6
.5
.4
.3
.2
.1
.0
7
6
5
4
3
2
1
0
0
4
8
12
16
20

Figure 8